Density Functional Study of the Mechanism of the Beckmann Rearrangement Catalyzed by H-ZSM-5: A Cluster and Embedded Cluster Study

Jakkapan Sirijaraensre,[†] Thanh N. Truong,*[,‡] and Jumras Limtrakul*[,†]

Computational and Applied Chemistry Laboratory, Physical Chemistry Division, Kasetsart University, Bangkok 10900, Thailand, and Henry Eyring Center for Theoretical Chemistry, Department of Chemistry, University of Utah, 315 S 1400 E, Room 2020, Salt Lake City, Utah 84112

Received: October 26, 2004; In Final Form: April 27, 2005

The mechanism of the Beckmann rearrangement (BR) catalyzed by the ZSM-5 zeolite has been investigated by both the quantum cluster and embedded cluster approaches at the B3LYP level of theory using the 6-31G-(d,p) basis set. Single-point calculations were carried out at the MP2/6-311G(d,p) level of theory to improve energetic properties. The embedded cluster model suggests that the initial step of the Beckmann rearrangement is not the O-protonated oxime but the N-protonated oxime. The energy barriers derived from the proton shuttle of the N-bound to the O-bound isomer are determined to be ∼99 and ∼40 kJ/mol for the embedded cluster and quantum cluster approaches, respectively. The difference in the activation energy is due mainly to the effect of the Madelung potential from the zeolite framework. The next step is the rearrangement step, which is the transformation of the O-protonated oxime to be an enol-formed amide compound, formimidic acid. The activation energy, at the rearrangement step, is calculated to be ∼125 and ∼270 kJ/mol for the embedded cluster and quantum cluster approaches, respectively. The final step is the tautomerization step which transforms the enol-form to the keto-form, formamide compound. The energy barrier for tautomerization is calculated to be 123 and 151 kJ/mol for the embedded cluster and quantum cluster approaches, respectively. These calculated results suggest that the rate-determining step of the vapor phase of the Beckmann rearrangement on H-ZSM-5 is the rearrangement or tautomerization step.

1. Introduction

The Beckmann rearrangement[1−6] is an industrially important reaction for the production of ϵ-caprolactam, a raw material for the production of Nylon-6, for which the market of consumption was 1 million tons in 1998.[7] Caprolactam is produced by the Beckmann rearrangement of cyclohexanone oxime with oleum, or concentrated sulfuric acid as a reaction medium. Although this procedure is convenient from a chemical standpoint, difficulties in manufacturing anticorrosion equipment and eliminating a large amount of the ammonium sulfate formed during the neutralization process make the process environmentally unacceptable. However, using a heterogeneous catalyst in this reaction, usually called the vapor phase of the Beckmann rearrangement, can circumvent these problems. Zeolite proves to be an excellent candidate[8−42] for taking over the catalytic function; thus, their use has benefits not only from an economical point of view but also from an ecological point of view.

The Beckmann rearrangement of the oxime compound has been widely investigated, especially on solid catalysts such as H-ZSM-5,[8−20] FAU,[21,22] B-ZSM-5,[25−28] etc. Fois et al.[17] studied the vapor phase of the Beckmann rearrangement in H-Faujasite, H-ZSM-5, and silicalite-1 by using IR spectroscopy and found that (a) both internal silanols and strong acid sites in zeolite can catalyze the Beckmann rearrangement of cyclohexanone oxime, (b) a stable protonated intermediate is formed on a strong acid site, and (c) the reaction at weak acid sites has a higher activation energy through a mechanism not involving a protonated intermediate. Ichihashi et al.[18] found that ZSM-5 was highly active for the Beckmann rearrangement when it had an Si/Al ratio of ≥500. Rhee et al.[23,24] studied the Beckmann rearrangement of cyclohexanone oxime over an H-β catalyst using FT-IR spectroscopy. They suggested that the initial step of the rearrangement involved the N-protonated complex of oxime, not the O-protonated complex.

Several theoretical studies on the mechanism of the Beckmann rearrangement in the gas phase have been reported.[17,43−47] Nguyen et al.[43−45] employed rather high levels of molecular orbital theories to examine the rearrangement of $CH_3-CH{=}N-OH$ oxime catalyzed by a proton, as a model of the BR under a strong acid condition. The Beckmann rearrangement was found to consist of two steps. The first step is 1,2-H-shift which connects the N-protonated complex and the O-protonated complex. The second step, denoted as the rearrangement step, is the concerted migration of the alkyl group to the nitrogen atom and elimination of a water molecule to produce a nitrilium cation. The first step was found to be the rate-determining step. Similar results were obtained by Fois et al. for the rearrangement of protonated cyclohexanone oxime. The latter study[17] also pointed out that, when a more realistic model for acidic condition was used, namely, a HCl molecule instead of H^+, a totally different mechanism was found. In fact, structures along the reaction coordinate were very different, and the rate-limiting step is the rearrangement step instead. The authors also modeled the BR catalyzed by silicalite by using a silanol molecule H_3-SiOH as a model. It was found that silanol cannot protonate the oxime; however, the rearrangement step is similar to that of the HCl−oxime complex and is also the rate-limiting step.

* To whom correspondence should be addressed. E-mail: fscijrl@ku.ac.th (J.L.) or truong@chem.utah.edu (T.N.T.).
[†] Kasetsart University.
[‡] University of Utah.

10.1021/jp045135w CCC: $30.25
Published on Web 06/01/2005

A conclusion by the authors is that the BR can follow different mechanisms on zeolites depending on the acidity of the Brønsted acid proton and silanol active centers. To the best of our knowledge, there has not been any theoretical study on the mechanism of the BR in a real zeolite framework. Such a study would be fundamentally important in providing more insight into the mechanism of the BR catalyzed by zeolites.

In this study, we performed a systematic theoretical investigation on the mechanism of the gas phase Beckmann rearrangement in ZSM-5 zeolite. The formaldehyde oxime was chosen as a model. Our objectives are (1) to understand the nature of the adsorption of formaldehyde oxime on H-ZSM-5 (i.e., can the Brønsted proton protonate the oxime, and if so, which form, N-protonated or O-protonated, would be more stable?), (2) to determine structures and energetic properties along the reaction pathway for the rearrangement, and thus the rate-limiting step of the reaction, and (3) to investigate the effects of the zeolite framework, particularly the effect of the Madelung potential, on the mode of adsorption of oxime and the mechanism of the BR process. To do so, we have employed both the bare cluster and embedded cluster approaches within the density functional theory.

2. Methods

ZSM-5 has 12 unique tetrahedral (T) sites where an aluminum atom can substitute for the Si atom in the framework to form a Brønsted acid site. In this study, the active site is assumed to be the T12 site since it was predicted to be among the most stable Al substitution sites,[36−42] and has been used to model the active site of ZSM-5 in many theoretical studies. In addition, it is located at the intersection of the main and sinusoidal channels, and thus, it is accessible to adsorbates. In our recent study,[37] we have tested model dependency on similar embedded cluster models of the ZSM-5 zeolite and found that there are two main factors that can affect the accuracy of the results, namely, the size of the QM cluster and the representation of the Madelung potential. However, it is difficult to separate the effects of these two factors. As the size of the QM cluster increases, it includes the short-range electrostatic, repulsion−dispersion, and polarization contributions from the local region of the active site in its full quantum mechanical treatment. Therefore, in principle, the larger model would provide the more accurate results, although the very large model would have limited use because of its computational demand. We found that the embedded 10T cluster model, in which the quantum 10T cluster represents a complete 10-membered ring of the main channel of ZSM-5, enclosing an active site and adsorbates, is sufficient for studying adsorption of molecules with binding energies of less than 60 kcal/mol; thus, it would be adequate for the systems considered here. The hybrid density functional theory B3LYP level was used. Because of the size of the cluster, we used a mixed basis set to represent the whole system. In particular, the 6-31G(d,p) basis set was used for the active site region [$H_2Si1OAl(OH)_2O(H)Si2H_2$] and the adsorbate while a smaller 3-21G basis set was used for the remaining part of the cluster. In an attempt to improve the energetic properties, single-point energy calculations were carried out at the MP2 level of theory using the 6-311G(d,p) basis set for the whole system.

To include the effects of the static Madelung potential from the remaining infinite lattice of zeolite (excluding the 10T quantum cluster), we employed the embedded cluster model[48] known as the surface charge representation of external electrostatic potential (SCREEP) method proposed by Stefanovich and Truong.[49,50] In this model, such an external Madelung potential

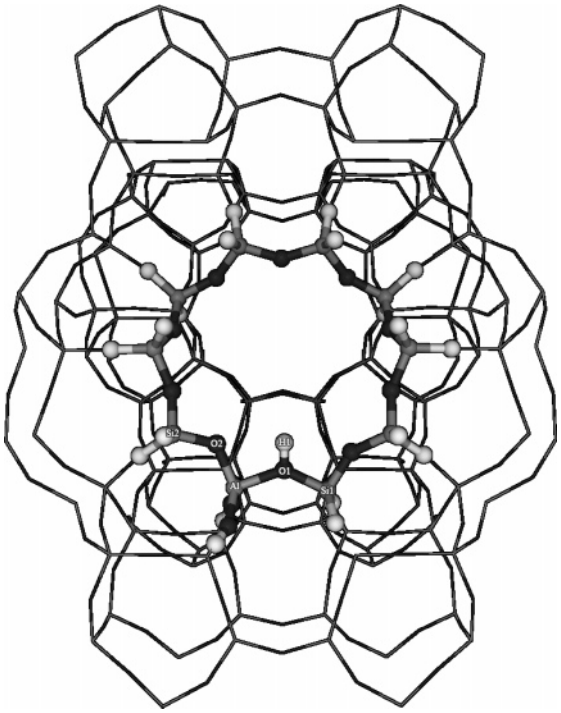

Figure 1. Optimized structures of the 10T cluster and embedded cluster of H-ZSM-5 zeolite at the B3LYP/6-31G(d,p) level of theory (values in parentheses are taken from the bare cluster).

can be represented by two sets of point charges. The potential from the unit cells that are closest to the quantum cluster is represented by point charges located at the lattice sites, while the remaining component is represented by a set of surface charges determined from the SCREEP method. Previous studies found the calculated adsorption properties agree well with experimental estimates,[36,37] suggesting that the SCREEP embedded approach is a sufficiently accurate and practical model for studying reaction mechanisms on zeolites.

In this work, in all geometrical optimizations, only the capping hydrogen atoms are fixed to be along the lattice Si−O bonds. Normal-mode analyses were performed to verify that the optimized transition state does connect the intended reactant and product. All calculations were performed using Gaussian98.[51] Calculations were done using computer resources at the Laboratory for Computational and Applied Chemistry (LCAC) at Kasetsart University.

3. Results and Discussion

3.1. Brønsted Acidic Site. Selected optimized bond lengths in the active site region are displayed in Figure 1. Values in parentheses are from the bare cluster calculations. When the results from the cluster and embedded cluster models are compared, the Madelung potential has the effect of lengthening the O1−H1 bond distance (Brønsted acid site) from 97.0 to 97.7 pm and shortening the adjacent Al−O bond, which is in accordance with Gutmann's rules.[52] In addition, the Mulliken population on the H1 atom is slightly increased from 0.38 to 0.41, indicating that the Brønsted proton is more acidic due to the Madelung potential effect. From our previous calculations on smaller clusters, we found that the structure of the Brønsted site is not very sensitive to cluster size. However, in this study, the 10T cluster is needed to accurately describe short-range electrostatic, repulsion−dispersion, and polarization interactions between the local region surrounding the active site and the adsorbate.

TABLE 1: Optimized Geometries and Adsorption Energies, ΔE_{ads} (kilojoules per mole), for N Complexes and O Complexes in the Bare Clusters and Embedded Cluster at the B3LYP/6-31G(d,p) Level of Theory (distances in picometers and angles in degrees)

	N complexes		O complexes	
parameter	10T cluster	10T embedded	10T cluster	10T embedded
O1−H1	154.2	177.1	101.2	139.6
N−H1	109.0	104.8	−	−
N−O1	262.0	279.2	−	−
O5−H1	−	−	164.8	108.1
O5−O1	−	−	261.5	245.7
O2−H2	153.2	170.3	173.2	189.8
H2−O5	98.6	99.7	98.6	99.2
O2−O5	254.0	268.1	257.4	266.4
N−O5	134.1	134.6	140.8	151.1
N−C	127.7	127.5	127.3	126.9
∠O1−H1−N	168.9	163.7	−	−
∠O2−H2−O5	165.7	165.7	−	−
∠O1−H1−O5	−	−	158.0	165.3
∠O2−H2−O5	−	−	141.0	131.8
∠O1−O2−O5−N	165.8	165.8	133.0	98.2
ΔE_{ads}	−135	−195	−86	−116
	−138[a]	−202[a]	−103[a]	−125[a]
	−114[b]	−176[b]	−85[b]	−113[b]

[a] Obtained at the MP2//B3LYP level of theory. [b] Obtained at the MP2/6-311G(d,p)//B3LYP level of theory.

3.2. Adsorption Complexes of Formaldehyde Oxime. There are two possible configurations of the adsorbed formaldehyde oxime (CH_2NOH) for interacting with the Brønsted proton (H1). One is where H1 forms a hydrogen bond with the nitrogen atom of the oxime in what is termed the N-bound configuration, and the other is one in which H1 forms a hydrogen bond with the OH group to form the O-bound configuration. The key issue is whether the Brønsted site is able to protonate the adsorbed formaldehyde oxime.

Selected optimized geometrical parameters and adsorption energies for the N-bound complex calculated using both the bare and embedded cluster models are listed in Table 1. For simplicity in the discussion below, all energetic information is determined at the MP2/6-311G(d,p)//B3LYP level of theory, unless otherwise specified. Selected bond lengths are also shown in Figure 2a to facilitate the discussion. Both models predict that the N-bound complex is protonated. The adsorbed protonated complex forms two hydrogen bonds (O1···H1 and O2···H2) in a seven-membered ring configuration where the oximes are nearly in the same plane with the 10T ring (the O1−O2−O5−N dihedral angle is 166°; see also Figure 2a). The adsorption energy is predicted to be −176 kJ/mol from the embedded cluster model. Note that it is much larger than the value of −114 kJ/mol from the bare cluster model. This indicates that the effects of the Madelung potential are significant. In fact, the N-protonated oxime appears to be more ionic, as indicated by the total Mulliken population on the protonated $[CH_2N\mathbf{H}OH]^+$ subunit of 0.76 from the embedded cluster model as compared to that of 0.67 from the bare cluster model. It is interesting to note that the Madelung potential further separates the protonated oxime moiety from the zeolite framework as the O1−H1 and O2−H2 bond distances were elongated by ∼20 pm. This effect is similar to the solvation of an ion pair complex. Similarly, the results for the O-bound complex are also shown in Table 1 and Figure 2b. Here we observed even larger effects of the Madelung potential from the zeolite framework. In fact, it promotes protonation of the O-bound complex. This is evident in the fact that only a molecular adsorbed state was found using the bare cluster model, whereas only the protonated complex was found using the embedded cluster model. The adsorbed protonated O-bound complex also forms two hydrogen bonds with the two bridging oxygen atoms, O1 and O2, of the zeolite framework, but in a six-membered ring configuration, where the oxime fragment is almost perpendicular to the plane of the 10T ring (the O1−O2−O5−N dihedral angle is 98°; see also Figure 2b). The adsorption energy of the protonated O-bound complex is −113 kJ/mol. Despite the Madelung potential inducing changes in the adsorption mode of the O-bound complex, it has a smaller increase in adsorption energy (28 kJ/mol) as compared to the value of 62 kJ/mol observed for the N-bound complex.

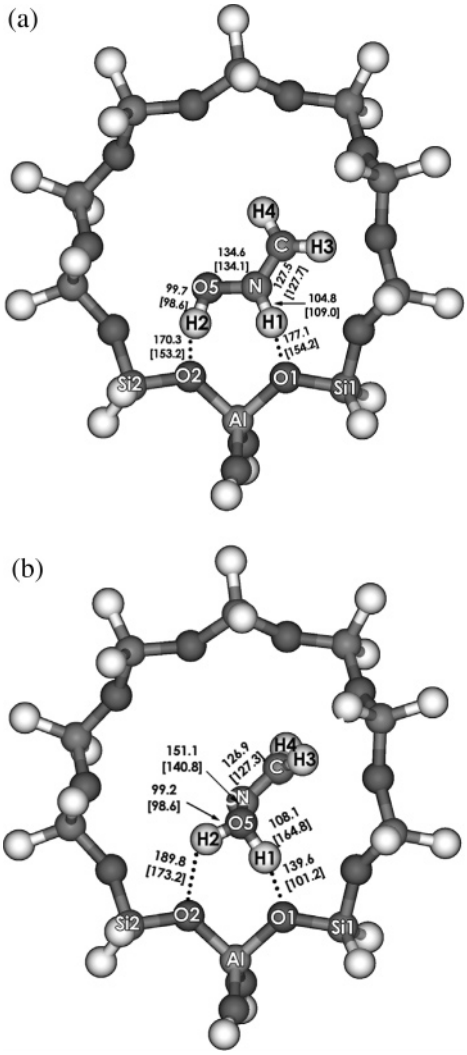

Figure 2. Optimized adsorption complexes on the 10T cluster and embedded cluster of H-ZSM-5 zeolite at the B3LYP/6-31G(d,p) level of theory: (a) N-bound complexes and (b) O-bound complexes (values in parentheses are taken from the bare cluster).

The protonated N-bound complex is much more stable than the protonated O-bound species by 63 kJ/mol as determined with the embedded model, which can be compared to the value of 77 kJ/mol in the isolated protonated formaldehyde oxime system. This result suggests that the initial structure of the Beckmann rearrangement is the protonated N-bound oxime. This finding is consistent with experimental observations by Fois et al.[17] and Chung and Rhee.[23,24] The bare cluster model also predicts the N-protonated complex is more stable than the O-bound complex but only by 29 kJ/mol. This indicates that the Madelung potential has a larger degree of stabilization for the N-bound complex. However, as pointed out in previous

TABLE 2: Optimized Geometries and Adsorption Energies, ΔE_{ads} (kilojoules per mole), for the 1,2-H-Shift Transition State in the 10T Bare Cluster and Embedded Cluster at the B3LYP/6-31G(d,p) Level of Theory (distances in picometers and angles in degrees)

parameter	10T cluster	10T embedded
O1−H1	98.2	100.3
N−H1	220.6	193.4
O5−H1	216.0	202.6
O5−O1	308.4	298.8
N−O1	306.8	283.7
H2−O5	98.5	97.6
H2−O2	180.0	202.7
O2−O5	272.6	288.3
N−O5	140.9	143.0
N−C	127.3	127.3
∠O1−H1−N	145.7	148.4
∠O1−H1−O5	156.1	160.0
∠O2−H2−O5	155.2	145.3
∠O1−O2−O5−N	58.9	60.2
ΔE_{ads}	−65	−67
	−84[a]	−82[a]
	−74[b]	−77[b]

[a] Obtained at the MP2//B3LYP level of theory. [b] Obtained at the MP2/6-311G(d,p)//B3LYP level of theory.

theoretical studies, the N-bound complex does not lead directly to the Beckmann rearrangement. It must first transform to the O-bound complex. The mechanism for such a process is discussed below.

3.3. Mechanism of the Beckmann Rearrangement. The mechanism of the Beckmann rearrangement of formaldehyde oxime on H-ZSM-5 zeolite consists of three steps. The first step is the 1,2-H-shift, which is the transformation from the N-bound configuration structure to the O-bound configuration structure. The second step is the rearrangement of the O-bound oxime complex to the amide complex, in which a hydrogen atom is transferred from the CH_2 group to the nitrogen atom and a water molecule is displaced. The next step is the water binding to the carbon atom, and then transferring a hydrogen atom to the NH group to form the intermediate product. The last step is tautomerization from the intermediate product to the amide product. The general feature of the potential energy surface for the first two steps is similar to the results obtained by Nguyen et al. for the protonated formaldehyde oxime system; however, there are distinct differences as discussed below. The schematic energy profile reported by Fois et al. also consists of three steps. Unfortunately, no structural information along the reaction path was reported, thus making more detailed comparisons difficult.

For the first step, the 1,2-hydrogen shift, the optimized structure of the transition state is illustrated in Figure 3a, and selected geometrical parameters and relative energies with the reference point being the infinitely separated oxime and zeolite are given in Table 2. The nature of the 1,2-H-shift for isomerization between the N-protonated oxime and the O-protonated oxime in ZSM-5 is very different when compared to that in the isolated protonated oxime system. In the isolated protonated oxime system, as studied by Nguyen et al., the transition state for the 1,2-H-shift has a rather tight structure where the active N−H and O−H bonds are less than 125 pm in length, whereas the transition state in the ZSM-5 zeolite has a rather loose structure where these active bonds are longer than 193.4 pm. In fact, at the transition state, the formaldehyde oxime is not protonated by ZSM-5 since the O1−H1 bond is only ∼100.3 pm in length. Thus, the zeolite framework assists the 1,2-H-shift step by forming a neutral hydrogen bond complex rather than the ion pair complex, thus relieving most of the structural constraints seen in the tight transition state of the isolated protonated case. Consequently, the barrier for this step in ZSM-5 is only 99 kJ/mol from the embedded model as compared to 225 kJ/mol in the isolated protonated system reported by Nguyen et al. The bare cluster model predicts the barrier for this step to be only 40 kJ/mol. This indicates that the Madelung potential from the zeolite framework has a much larger degree of stabilization of the N-bound protonate oxime than at the transition state.

TABLE 3: Optimized Geometries and Adsorption Energies, ΔE_{ads} (kilojoules per mole), for the Rearrangement Step in the 10T Bare Cluster and Embedded Cluster at the B3LYP/6-31G(d,p) Level of Theory (distances in picometers and angles in degrees)

	rearrangement transition state		formimic acid complex	
parameter	10T cluster	10T embedded	10T cluster	10T embedded
O1−H1	193.6	232.4	101.3	113.6
O5−H1	98.5	97.4	157.5	129.7
O2−H2	176.4	205.4	196.6	209.3
O5−H2	99.3	97.6	98.5	98.0
O5−O1	275.6	309.9	256.6	242.2
O5−O2	270.2	293.0	265.1	269.1
N−O5	217.9	228.3	−	−
N−O2	400.0	475.4	428.1	427.4
N−H4	117.9	129.2	102.0	102.0
N−C	120.0	119.3	126.0	125.0
C−H3	111.4	110.5	109.3	108.9
C−H4	136.5	128.3	−	−
C−O5	−	−	136.4	139.7
∠C−N−O5	108.3	100.8	−	−
∠N−C−O5	−	−	120.6	117.9
∠O1−H1−O5	139.0	136.0	164.6	168.9
∠O2−H2−O5	156.1	148.4	124.4	117.6
ΔE_{ads}	187	26	−249	−264
	168[a]	0[a]	−276[a]	−289[a]
	185[b]	12[b]	−260[b]	−276[b]

[a] Obtained at the MP2//B3LYP level of theory. [b] Obtained at the MP2/6-311G(d,p)//B3LYP level of theory.

The optimized geometry of the transition state for the rearrangement step is shown in Figure 3b, with selected geometrical parameters and relative energies given in Table 3, along with the information for the intermediate, HNCH-OH···HZ complex. The optimized geometry of the adsorbed formimidic acid complex is also given in Figure 3c. The rearrangement step consists of a concerted 1,2-H-shift from the CH_2 group to the nitrogen atom accompanied by the release of a water molecule from the cleavage of the N−O bond. The transition state geometry qualitatively resembles that from the previous study on the protonated formaldehyde oxime. However, quantitatively there are differences; namely, the transition state for the reaction in zeolite is closer to the product side than that in the isolated system. In particular, for the reaction in zeolite the migrating hydrogen atom, H4, is at the midway point between the C and N atoms (C−H4 and N−H4 bond distances are 128.3 and 129.2 pm, respectively), whereas it is still much closer to the reactant side for the isolated protonated oxime system (C−H and N−H active bond distances are 119.2 and 142.4 pm, respectively). The breaking N−O bond is also longer for the reaction in zeolite (228.3 vs 205.6 pm). The calculated barrier for this step is 125 kJ/mol from the embedded model, which is almost 80 kJ/mol higher than the previously reported value of 44 kJ/mol for the isolated protonated oxime system. Comparing results between the embedded and bare cluster models, we found that the Madelung potential noticeably shifts

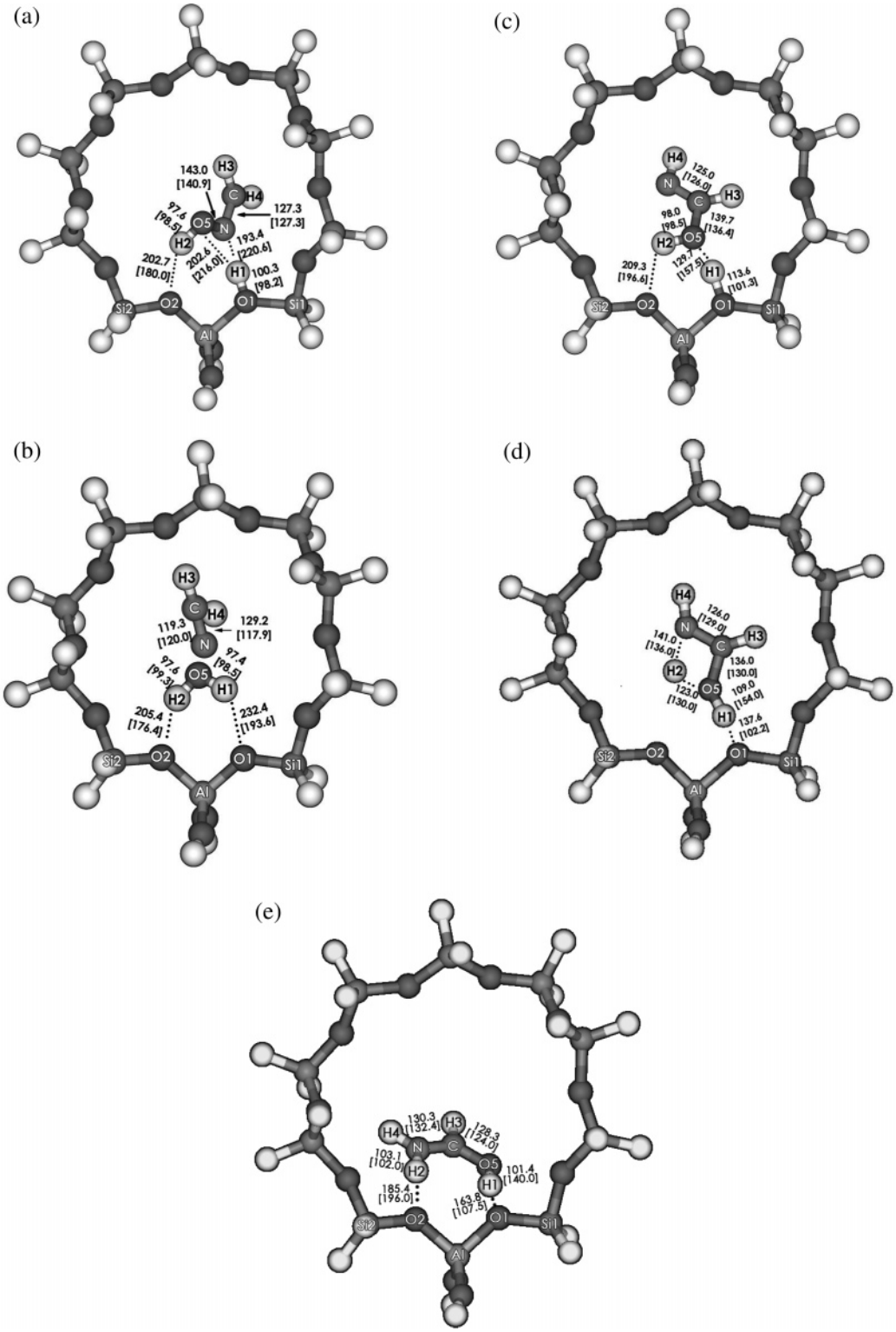

Figure 3. Optimized complexes on 10T H-ZSM-5 zeolite at the B3LYP/6-31G(d,p) level of theory: (a) 1,2-H-shift transition state complexes, (b) Beckmann rearrangement transition state complexes, (c) formimidic acid complexes, (d) tautomerization transition state complexes, and (e) formamide complexes (values in parentheses are taken from the bare cluster).

the transition state toward the primary product. The effect of the Madelung potential on the barrier height of this step, however, is much stronger. In particular, it lowers the activation energy by 145 kJ/mol.

However, the final product of the Beckmann rearrangement reaction of formaldehyde oxime is not formimidic acid (HNCHOH), which is the primary product obtained from the rearrangement step, but formamide (H_2NCHO). The final step is the tautomerization of the primary product, the formimidic acid complex (HNCHOH···HZ complex), to the more stable product, the formamide complex (H_2NCHO···HZ complex), by migrating the hydrogen atom (H2) from the oxygen atom (O5) to the nitrogen atom (N). The optimization geometry of the transition state for the tautomerization step is shown in Figure 3d, and selected geometrical parameters are given in Table 4. The transferring proton (H2) is at the midway point between the O5 and N atoms (N−H2 and O2−H2 bond distances of 141.0 and 123.0 pm, respectively), which happens simulta-

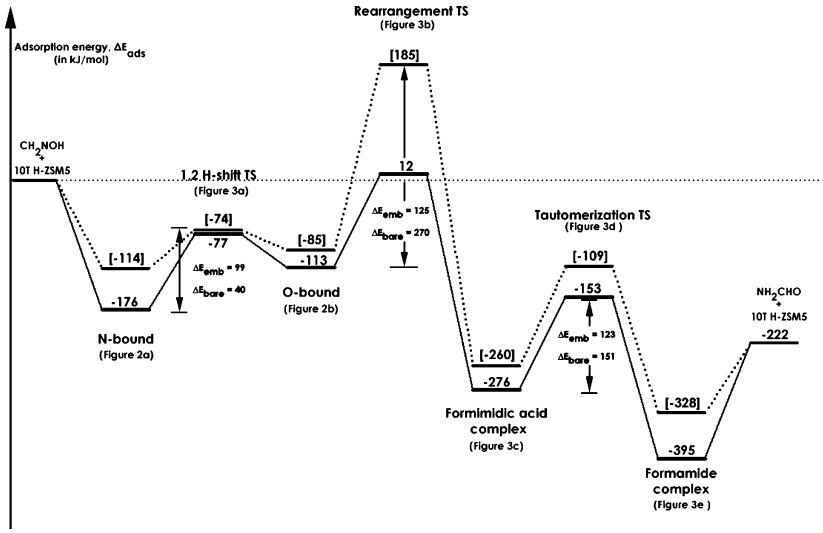

Figure 4. Energetic profile along the Beckmann rearrangement pathway of formaldehyde oxime adsorbed on 10T H-ZSM-5 zeolite at the MP2/6-311G(d,p)//B3LYP level of theory. The energetic changes for the embedded cluster (solid line) and the bare cluster (dotted line) complexes are in kilojoules per mole.

TABLE 4: Optimized Geometries and Adsorption Energies, ΔE_{ads} (kilojoules per mole), for the Tautomerization Step in the 10T Bare Cluster and Embedded Cluster at the B3LYP/6-31G(d,p) Level of Theory (distances in picometers and angles in degrees)

	tautomerization transition state		formamide complex	
parameter	10T cluster	10T embedded	10T cluster	10T embedded
O1−H1	102.2	137.6	107.5	163.8
O5−H1	154.0	109.0	140.0	101.4
O2−H2	−	−	196.0	185.4
O5−H2	130.0	123.0	−	−
O5−O1	256.7	245.3	247.0	264.6
O5−O2	287.2	288.2	343.4	368.7
N−O2	428.3	403.1	294.9	286.7
N−H4	101.0	101.0	100.0	101.2
N−H2	136.0	141.0	102.0	103.1
N−C	129.0	126.0	132.4	130.3
C−H3	108.0	108.0	109.0	108.9
C−O5	130.0	136.0	124.0	128.3
∠N−C−O5	106.8	103.7	125.5	124.7
∠O1−H1−O5	174.2	167.4	168.6	171.5
∠O5−H2−N	103.0	102.8	62.2	61.8
∠O1−O2−N−O5	−	−	6.1	13.7
ΔE_{ads}	−108	−169	−327	−393
	−130[a]	−174[a]	−346[a]	−408[a]
	−109[b]	−153[b]	−328[b]	−395[b]

[a] Obtained at the MP2//B3LYP level of theory. [b] Obtained at the MP2/6-311G(d,p)//B3LYP level of theory.

neously with the slight shortening of the C−O5 bond and the elongating of the N−C bond for shifting to the amide compound. However, comparing the tautomerized transition state structure between both models, we found that the protonation occurred concurrently during tautomerization in the embedded cluster model. The O1−H1 bond was elongated by ∼35 pm to form an O−H single bond. The energy barrier for this step is predicted to be 123 kJ/mol by using the embedded cluster model. The effect of the Madelung potential from the zeolite framework slightly lowers the activation energy as compared to that obtained from the bare cluster model. The results agree well with previous studies which have investigated in the same reaction for other different molecules such as *N*-nitrobenzene sulfonamides,[53] isocyanates,[54] β-lactams,[55] carbodiimine,[56] and acetamide.[57] The activation energy for the tautomerization step of these molecules is ∼105−125 kJ/mol. Compared to the activation energy for the previous rearrangement step, it is slightly lower, and thus, both of these rearrangement steps could be the rate-limiting step for the whole mechanism.

Finally, the final product of the reaction is formamide. The optimized geometry of the adsorbed formamide complex is given in Figure 3e. From the embedded cluster model, the adsorbed protonated formamide, $[H_2NC(O\mathbf{H})H]^+$, forms two strong hydrogen bonds to both $C{=}O^+{-}H$ and NH_2 groups which interact with the two bridging oxygen atoms, O1 and O2, of the zeolite framework in the six-membered ring configuration, whereas only the neutral formed complex was found using the bare cluster model. Both adsorption complexes that are obtained correspond with their transition state structures in the tautomerization step. The adsorption energy of protonated formamide is calculated to be −395 kJ/mol using the embedded

TABLE 5: Comparison of the Adsorption Energies, ΔE_{ads} (kilojoules per mole), along the Beckmann Rearrangement of Formaldehyde Oxime on 10T H-ZSM-5 Zeolite in Bare Cluster and Embedded Cluster Models by Different Methods[a]

	ΔE_{ads}		
	B3LYP	MP2//B3LYP	MP2/6-311G(d,p)//B3LYP
N-bound complex	−195 [−135]	−202 [−138]	−176 [−114]
1,2-H-shift transition state complex	−67 [−65]	−82 [−84]	−77 [−74]
O-bound complex	−116 [−86]	−125 [−103]	−113 [−85]
rearrangement transition state	26 [187]	0 [168]	12 [185]
enol−amide complex	−264 [−249]	−289 [−276]	−276 [−260]
tautomerization transition state	−169 [−108]	−174 [−130]	−153 [−109]
keto−amide complex	−393 [−327]	−408 [−346]	−395 [−328]

[a] Values in brackets were obtained with the bare cluster model.

cluster model. In a comparison of the optimized structure which was obtained from both models with the isolated formamide, the structure of adsorbed formamide provides the lengthening of the C−O bond distance (by 2.4 and 6.7 pm for the bare and embedded clusters, respectively) and shortening of the C−N bond distance (by 4.1 and 5.8 pm for the bare and embedded clusters, respectively). The C−O bond length presents single-bond character, while the C−N bond length shows double-bond character, similar to that observed by Cho et al.[58] Changing of the C−O and C−N bond lengths is due mainly to the mesomeric effects resulting from the donation of the lone pair of electrons from the nitrogen atom that pass through the π-bond of the C═O bond to give a different resonance of formamide. In this study, it seems that the framework effect which is represented by the Madelung potential plays an important role in the stabilization of the protonated N,O-formaldehyde oxime and formamide configurations, which is the crucial step in allowing the Beckmann rearrangement to occur.

The effects of the Madelung potential of the extended zeolite framework on the energetic and mechanism of this reaction can also be seen from Figure 4. In particular, the Madelung potential tends to stabilize the stable intermediates by 16−67 kJ/mol. It also lowers the activation energies for all steps involved in this mechanism. The largest effect is at the rearrangement step from the O-bound oxime to the formimidic acid (Figure 2b and Figure 3c), where the Madelung potential lowers the activation energy by 145 kJ/mol. Consequently, it makes this rearrangement step have an activation energy comparable with that of the tautomization from formimidic to formamide (Figure 3c,e); thus, either could be the rate-limiting step.

4. Conclusions

The vapor phase of the Beckmann rearrangement of formaldehyde oxime over the zeolite ZSM-5 catalyst has been studied by both the bare cluster and embedded cluster methods at the B3LYP/6-31G(d,p) level of theory. The N-protonated species was obtained in both the cluster and embedded cluster methods. Using the cluster model (10T), the complex obtained by the latter method is more stable than that from the former by ∼60 kJ/mol. For the interaction of zeolite with the oxygen atom of oxime (O-oxime) molecules, the cluster models yielded only hydrogen-bonded adducts, while the O-protonated species was only obtained with the 10T embedded method. This embedded result indicates that the N-protonation of oxime is preferable to the O-protonation. This study suggests that the initial structure of the Beckmann rearrangement reaction is not the O-protonation but the N-protonation of oxime. The energy barrier for the 1,2-H-shift connecting N- and O-protonated species is lower than that of the rearrangement and tautomerization steps. From the calculations, one can conclude that the rate-determining step of the reaction is either the rearrangement or tautomerization step which has an energy barrier of ∼125 kJ/mol. Furthermore, we found that the extended framework significantly affects the results of protonation of the formamide molecule. Our finding may be good supporting evidence for the newly proposed mechanism for the cyclohexanone oxime that interacts with zeolites and finding the suitable zeolite for this reaction. This indicates that inclusion of the effects of the zeolite crystal framework is crucial for obtaining the mechanistic aspect of the Beckmann rearrangement.

Acknowledgment. This research has been supported in part by a TRF Senior Research Scholar from the Thailand Research Fund, The Ministry of University Affairs under the Science and Technology Higher Education Development Project (MUA-ADB funds), the Kasetsart University Research and Development Institute (KURDI), a Grant-in-Aid for Thesis from the Graduate School, Kasetsart University, to J.S. and an ACS Petroleum Research Fund grant to T.N.T.

References and Notes

(1) Beckmann, E. *Chem. Ber.* **1886**, *89*, 988.
(2) Blatt, A. H. *Chem. Rev.* **1933**, *12*, 215.
(3) Jones, B. *Chem. Rev.* **1944**, *35*, 335.
(4) Heldt, W. Z. *J. Org. Chem.* **1961**, *26*, 1695.
(5) Ungnade, H. E.; McLaren, A. D. *J. Org. Chem.* **1945**, *10*, 29.
(6) Pearson, D. E.; Bruton, J. D. *J. Org. Chem.* **1954**, *19*, 957.
(7) *European Chemical News*; Haywards: Heath, U.K., 1999; Vol. 18.
(8) Takahashi, T.; Nishi, M.; Tagawa, Y.; Kai, T. *Microporous Mater.* **1995**, *3*, 467.
(9) Takahashi, T.; Ueno, K.; Kai, T. *Microporous Mater.* **1993**, *1*, 323.
(10) Heitmann, G. P.; Dahlhoff, G.; Hölderich, W. F. *J. Catal.* **1999**, *186*, 12.
(11) Ichihashi, H.; Kitamura, M. *Catal. Today* **2002**, *73*, 23.
(12) Yashima, T.; Oka, N.; Komatsu, T. *Catal. Today* **1997**, *38*, 249.
(13) Kath, H.; Gläser, R.; Weitkamp, J. *Chem. Eng. Technol.* **2001**, *24*, 150.
(14) Misona, M.; Inui, T. *Catal. Today* **1999**, *51*, 369.
(15) Takahashi, T.; Nasution, M. N. A.; Kai, T. *Appl. Catal., A* **2001**, *210*, 339.
(16) O'Sullivan, P.; Forni, L.; Hodnett, B. K. *Ind. Eng. Chem. Res.* **2001**, *40*, 1471.
(17) Fois, G. A.; Ricchiardi, G.; Bordiga, S.; Busco, C.; Dalloro, L.; Spano, G.; Zecchina, A. *Stud. Surf. Sci. Catal.* **2001**, *135*, 2477.
(18) Ichihashi, H.; Sato, H. *Appl. Catal., A* **2001**, *221*, 359.
(19) Takahashi, T.; Kai, T.; Nakao, E. *Appl. Catal.* **2004**, *262*, 137.
(20) Forni, L.; Fornasari, G.; Giordano, G.; Lucarelli, C.; Katovic, A.; Triffiro, F.; Perri, C.; Nagy, J. B. *Phys. Chem. Chem. Phys.* **2004**, *6*, 1842.
(21) Dai, L. X.; Iwaki, Y.; Koyama, K.; Tatsumi, T. *Appl. Surf. Sci.* **1997**, *121−122*, 335.
(22) Dai, L. X.; Koyama, K.; Miyamoto, M.; Tatsumi, T. *Appl. Catal., A* **1999**, *189*, 237.
(23) Rhee, H. K.; Chung, Y. M. *J. Mol. Catal. A: Chem.* **2000**, *159*, 389.
(24) Rhee, H. K.; Chung, Y. M. *J. Mol. Catal. A: Chem.* **2001**, *175*, 249.
(25) Hölderich, W. F. *Catal. Today* **2000**, *62*, 115.
(26) Röseler, J.; Heitmann, G.; Hölderich, W. F. *Appl. Catal., A* **1996**, *144*, 319.
(27) Heitmann, G. P.; Dahlhoff, G.; Neiderer, J. P. M.; Hölderich, W. F. *J. Catal.* **2000**, *194*, 122.
(28) Hölderich, W. F.; Röseler, J.; Heitmann, G. P.; Liebens, A. T. *Catal. Today* **1997**, *37*, 353.
(29) Dal Pozzo, L.; Fornasari, G.; Monti, T. *Catal. Commun.* **2002**, *3*, 369.
(30) Paker, W. O., Jr. *Magn. Reson. Chem.* **1999**, *37*, 433.
(31) Komatsu, T.; Maeda, T.; Yashima, T. *Microporous Mesoporous Mater.* **2000**, *35−36*, 173.
(32) Ko, A. N.; Hung, C. C.; Chen, C. W.; Ouyang, K. H. *Catal. Lett.* **2001**, *71*, 219.
(33) Chaudhari, K.; Bal, R.; Chandwadkar, A. J.; Sivasanker, S. *J. Mol. Catal. A: Chem.* **2000**, *77*, 247.
(34) Shouro, D.; Ohya, Y.; Mishima, S.; Nakajima, T. *Appl. Catal., A* **2001**, *214*, 59.
(35) Singh, P. S.; Bandyopadhyay, R.; Hegde, S. G.; Rao, B. S. *Appl. Catal., A* **1996**, *136*, 249.
(36) Limtrakul, J.; Nanok, T.; Khongpracha, P.; Jungsuttiwong, S.; Truong, T. N. *Chem. Phys. Lett.* **2001**, *349*, 161.
(37) Treesukol, P.; Limtrakul, J.; Truong, T. N. *J. Phys. Chem. B* **2001**, *105*, 2421.
(38) Limtrakul, J.; Nokbin, S.; Chuichay, P. *J. Mol. Struct.* **2001**, *560*, 169.
(39) Limtrakul, J.; Nokbin, S.; Jungsuttiwong, S.; Khongpracha, P.; Truong, T. N. *Stud. Surf. Sci. Catal.* **2001**, *135*, 2469.
(40) Jungsuttiwong, S.; Nokbin, S.; Chuichay, P.; Khongpracha, P.; Truong, T. N.; Limtrakul, J. *Stud. Surf. Sci. Catal.* **2001**, *135*, 2518.
(41) Limtrakul, J.; Khongpracha, P.; Jungsuttiwong, S. *J. Mol. Struct.* **2000**, *525*, 153.
(42) Limtrakul, J.; Khongpracha, P.; Jungsuttiwong, S.; Truong, T. N. *J. Mol. Catal. A: Chem.* **2000**, *153*, 2469.
(43) Nguyen, M. T.; Raspoet, G.; Vanquickenborne, L. G. *J. Chem. Soc., Perkin Trans. 2* **1995**, *9*, 1791.
(44) Nguyen, M. T.; Raspoet, G.; Vanquickenborne, L. G. *J. Am. Chem. Soc.* **1997**, *119*, 2552.

(45) Nguyen, M. T.; Raspoet, G.; Vanquickenborne, L. G. *J. Chem. Soc., Perkin Trans. 2* **1997**, *4*, 821.

(46) Gomez, B.; Fuentealba, P.; Contreras, R. *Theor. Chem. Acc.* **2003**, *110*, 421.

(47) Ishida, M.; Suzuki, T.; Ichihashi, H.; Shiga, A. *Catal. Today* **2003**, *87*, 187.

(48) Vetrivel, R.; Catlow, C. R. A.; Colbourn, E. A. *Proc. R. Soc. London, Ser. A* **1988**, *417*, 81. (b) Aloisi, G.; Barnes, P.; Catlow, C. R. A.; Jackson, R. A.; Richard, A. J. *J. Chem. Phys.* **1990**, *93*, 3573. (c) Brandle, M.; Sauer, J. *J. Am. Chem. Soc.* **1998**, *120*, 1556. (d) Eichler, U.; Brandle, M.; Sauer, J. *J. Phys. Chem. B* **1997**, *101*, 10035. (e) Kyrlidis, A.; Cook, S. J.; Chakraborty, A. K.; Bell, A. T.; Theodorou, D. N. *J. Phys. Chem.* **1995**, *99*, 1505. (f) Teunissen, E. H.; Jansen, A. P. J.; van Santen, R. A. *J. Phys. Chem.* **1995**, *99*, 1873. (g) Teunisson, E. H.; Jansen, A. P. J.; van Santen, R. A.; Orlando, R.; Dovesi, R. *J. Chem. Phys.* **1994**, *101*, 5865. (h) White, J. C.; Hess, A. C. *J. Phys. Chem.* **1993**, *97*, 8730.

(49) Stefanovich, E. V.; Truong, T. N. *J. Phys. Chem. B* **1998**, *102*, 3018.

(50) Vollmer, J. M.; Stefanovich, E. V.; Truong, T. N. *J. Phys. Chem. B* **1999**, *103*, 9415.

(51) Frisch, M. J.; Trucks, G. W.; Schlegel, H. B.; Scuseria, G. E.; Robb, M. A.; Cheeseman, J. R.; Zakrzewski, V. G.; Montgomery, J. A.; Stratmann, R. E., Jr.; Burant, J. C.; Dapprich, S.; Millam, J. M.; Daniels, A. D.; Kudin, K. N.; Strain, M. C.; Farkas, O.; Tomasi, J.; Barone, V.; Cossi, M.; Cammi, R.; Mennucci, B.; Pomelli, C.; Adamo, C.; Clifford, S.; Ochterski, J.; Petersson, G. A.; Ayala, P. Y.; Cui, Q.; Morokuma, K.; Salvador, P.; Dannenberg, J. J.; Malick, D. K.; Rabuck, A. D.; Raghavachari, K.; Foresman, J. B.; Cioslowski, J.; Ortiz, J. V.; Baboul, A. G.; Stefanov, B. B.; Liu, G.; Liashenko, A.; Piskorz, P.; Komaromi, I.; Gomperts, R.; Martin, R. L.; Fox, D. J.; Keith, T.; Al-Laham, M. A.; Peng, C. Y.; Nanayakkara, A.; Challacombe, M.; Gill, P. M. W.; Johnson, B.; Chen, W.; Wong, M. W.; Andres, J. L.; Gonzalez, C.; Head-Gordon, M.; Replogle, E. S.; Pople, J. A. *Gaussian'98*; Gaussian, Inc.: Pittsburgh, PA, 2001.

(52) Gutmann, V. *The donor−acceptor approach to molecule interactions*; Plenum Press: New York, 1978.

(53) Cox, R. A. *J. Chem. Soc., Perkin Trans.* **1997**, *2*, 1743.

(54) Raspoet, G.; Nguyen, M. T.; McGarraghy, M.; Hegarty, A. F. *J. Org. Chem.* **1998**, *63*, 6867.

(55) Pitarch, J.; Ruiz-Lopez, M. F.; Silla, E.; Pauscual-Ahuir, J. L.; Tunon, I. *J. Am. Chem. Soc.* **1998**, *120*, 2146.

(56) Lewis, M.; Glaser, R. *J. Am. Chem. Soc.* **1998**, *120*, 8541.

(57) Barbosa1, L. A. M. M.; van Santen, R. A. *J. Catal.* **2000**, *191*, 200.

(58) Cho, S. J.; Cui, C.; Lee, J. Y.; Park, J. K.; Suh, S. B.; Park, J.; Kim, B. H.; Kim, K. S. *J. Org. Chem.* **1997**, *62*, 4068.